Table of Contents

Production-based emission inventory

Detailed sectoral disaggregation of production-based emissions is necessary for tracking the emissions embodied in internationally-traded goods and services; however, available global inventories usually provided industrial emissions at aggregated level. Thus, we developed an alternate global inventory of carbon monoxide (CO), sulfur dioxide (SO_2), nitrogen oxides (NO_x), black carbon (BC), and organic carbon (OC) emissions for the year 2007. This inventory is also used to support another study that examines the direct forcing of aerosols embodied in international trade[34]. We estimate emissions from all major anthropogenic sources except open biomass burning (but including biofuels). Global anthropogenic emissions in 2007 are estimated as follows: 101.7 Tg SO_2, 95.3 Tg NO_x, 532.1 Tg CO, 5.8 Tg BC, and 13.7 Tg OC. For NH_3 emissions, we adopt the emission data from EDGAR v4.2[35] by coupling the MEIC inventory for China[36,37] and the USNEI for the U.S.[38]. The national annual SO_2, NO_x, CO, BC, OC, and NH_3 emissions estimates for the year 2007 are presented in Supplementary Fig. 1.

For species other than NH_3, emissions are estimated using a detailed technology-based methodology (Supplementary Fig. 2), which covers 62 subdivided sectors for 228 countries and regions. Methods and data used to compile the inventory are described below. We exclude NMVOC emissions from this analysis because large fractions of NMVOC emissions are emitted from activities (i.e. solvent use, fugitive emissions from fuels) that are difficult to ascribe to particular industry sectors. The NMVOC emissions used in the GEOS-Chem model thus remain constant across different scenario runs. We assessed the impact of excluding NMVOC from consumption-based analysis, and present those results below.

In deriving emissions for species other than NH_3, annual emissions for each species and country are estimated by:

$$E_{s,i} = \sum_m \sum_j A_{m,i,j} \left[\sum_f X_{m,i,j,f} EF_{s,m,i,j,f} \right] \tag{1}$$

where *s, m, i, j,* and *f* represent the species, emitting sectors, countries, fuel or product types, and technology type for combustion and industrial processes, respectively. *A* represents the activity rate, such as fuel consumption or material production. *X* represents the fraction of fuel or production that is consumed by a specific technology in a given sector, with $\sum X = 1$ for each fuel and sector. *EF* is the net emission factor.

For a given technology *f*, the net emission factor is estimated as:

$$EF = EF_{RAW} \sum_n C_n (1 - \eta_n) \tag{2}$$

where *n* represents a specific control technology, EF_{RAW} is the unabated emission factor. C_n is the penetration of control technology *n*, with $\sum C = 1$ for each technology. Finally, η_n is the removal efficiency of control technology *n*.

Activity rates. Country-specific fuel consumption data were obtained from the International Energy Agency (IEA)[39,40], which includes 51 fuels in 46 sub-sectors and four sectors (residential, industry, power, and transportation; field burning, international shipping, and international aviation are excluded). We aggregated this IEA fuel consumption data into

19 fuel types given that certain fuels lack emission factor information but are known to have minor emissions. Fuel consumption in each sub-sector is further divided by technologies (X in Eq. 1). For China and India, technology distributions are derived from the MEIC model[36,37] and Lu et al.[41] respectively. For other countries, technology distributions are taken from our previous work[42-44] and modified by estimates of residential biofuel combustion from the GAINS model[45] (http://gains.iiasa.ac.at/models) and estimates of transportation combustion from Yan et al.[46]. We also classified 16 non-combustion sources for the industrial process sector. Country-specific industrial production levels were obtained from public datasets, including United States Geological Survey statistics (USGS, http://minerals.usgs.gov/minerals/pubs/myb.html) developed by the National Minerals Information Center and United Nations data (http://data.un.org/). Ultimately, we classify activity rates into 62 sub-sectors, 19 fuel types, 16 products, and 38 technology combinations, with the detailed combinations and descriptions shown in Supplementary Table 2.

Emission factors. Emission factors used in this study were compiled from a large number of previous studies and previous work of some of this study's authors. Emission factors for transportation sector were obtained from Yan et al.[46,47]. The sources of emission factors for other sectors are documented below.

For SO_2, sulfur contents of fossil fuels were obtained from the GAINS model, USGS, and previous literatures[41,43,48-50]. The sulfur retention ratio was derived from USEPA AP-42[51] and other previous work[41,43,49]. SO_2 emission factors of biofuel combustion were based on the reported measurements[52,53] and USEPA AP-42[51]. For non-combustion sources, unabated SO_2 emission factors are directly obtained from publically available emission factor databases[51,54].

For NO_x, unabated emission factors were obtained from the literature[53,55-58], and public emission factor databases[51,54].

Unabated CO emission factors were acquired from USEPA AP-42[51] and Yevich et al.[59], and regional emission databases were then used to override global defaults where available[38,57,60-62].

For BC and OC, raw emission factors of combustion sources were obtained from Lei et al.[63] and Bond et al.[64,65]. Emission factors of residential kerosene were obtained from Lam et al.[66] and Huang et al.[67] Emission factors for industrial process were taken from the GAINS model. Emission factors for China and India were further replaced by our previous work[41].

Net emission factors were further determined by penetration rates and removal efficiencies of control technologies. Application rates of flue-gas desulfurization (FGD) devices and NO_x emission control technologies were obtained from literatures[41,43,48,57,68] and the GAINS model. Removal efficiencies for FGD and NO_x emission control technologies were derived from USEPA AP-42[51]. The penetration rates of fine particulate matter control device and corresponding removal efficiencies were obtained from Streets et al.[43] and Bond et al.[64]. In general, the high end of the removal efficiency ranges applies to the most developed regions, and the low end of the ranges applies to less developed regions. Local knowledge

from regional emission inventories[38,41,60-62,68,69] were then used to calibrate net SO_2 emission factors for China, India, Southeast Asia, Canada, the U.S., and Europe, respectively.

Statistics for emission uncertainty analysis. Emissions estimates are subject to uncertainty due to incomplete knowledge of activity rates and emission factors. To facilitate the uncertainty analysis later, here we briefly discuss assumptions in our estimate of uncertainties in production-based emissions. Following the approach documented by Streets et al.[55], we estimated uncertainties for each emitting sub-sector in the 13 world regions by combining the coefficients of variations (CV, or the standard deviation divided by the mean) of each contributing factor. The term "uncertainty" here refers to a 95% confidence interval around the central estimate (i.e. mean). Following Streets et al.[55], the CV of activity rates was determined by expert judgement supplemented with sources in the literature[42,64,70] since uncertainties are not provided in the statistics. We classified the 13 regions into three groups according to different levels of statistical infrastructure[28], and different levels of CV were assigned to each group. We assumed all CV of activity rates were normally distributed. The CV of emission factors were derived from available literatures[42,64,70] and the standard deviation of measurement data[53,71]. For emission factors derived from public emission factor databases, the emission factor rating A~E were transferred to CV of 0.05 to 5 and assumed to be distributed normally or lognormally. For NH_3, because emissions are compiled from several global and regional inventories, we estimated rough uncertainty ranges by using the sector- and region-specific uncertainties provided by Janssens-Maenhout et al.[28].

Comparison with HTAP v2.2 global inventory. HTAP v2.2[28] was developed for the TF HTAP by harmonizing EDGAR v4.3 global inventory and several regional inventories including official inventories for U.S.[38] and Canada[62], EMEP[61] and TNO[72] for Europe, and MIX for Asia[37]. Thus, the HTAP v2.2 inventory represents the state-of-the-art understanding of global emissions since it combines latest available regional information into a complete and consistent global dataset. Comparing our emission inventory (year 2007) with HTAP v2.2 (year 2008), we found that sectoral and regional estimates of the two datasets generally agree well, with differences that are generally within the uncertainty ranges for these types of bottom-up inventories (Supplementary Fig. 3). The different reference year (2007 vs. 2008) accounts for some of the observed differences between two datasets. Taking SO_2 emissions from energy sectors in Western Europe as an example, estimates in HTAP v2.2 are 49% lower than in this work, in line with 47% decrease of emissions between 2007 and 2008 due to the financial crisis[61]. By comparing the emissions in the two datasets for each of 129 GTAP regions[34], the agreement of the two datasets is further evidenced by correlation coefficients that fall between 0.98-1.00 across different pollutants and a normalized mean bias (NMB) from 0.2% to 18%.

Tracing production-based emissions to their consumption destinations

Consumption-based emissions refer to air pollutants produced throughout the supply chain as a result of certain consumption activity[73,74]. For example, the goods and services consumed in the U.S. may entail manufacturing of parts, assembly and transport in multiple regions worldwide, with attendant air pollution emissions in those other regions. We used a multi-regional input-output model (MRIO) (Extended Data Fig. 7) to capture these complex economic interconnections among sectors and regions[75] and assign the emissions produced throughout the supply chains to the region where the finished goods are ultimately consumed. Based on detailed trade data about the exchange of goods and services among different industry sectors, the MRIO allocates all the emissions related to a given consumption activity to the final consumer. For example, an electronic appliances consumed in the U.S., and assembled in China from goods manufactured in Vietnam will embody emissions from the energy sector in Vietnam in proportion to the energy used to manufacture the parts, as well as emissions from the energy sector in China in proportion to the energy used during assembly and transport. The MRIO model used in this study is the same as that constructed by Andrew and Peters[31,32] using data from version 8 of the Global Trade Analysis Project (GTAP)[33]. Using the MRIO, emissions produced in each region can be quantitatively decomposed into the components related to consumption activities in other regions and domestically. Previous studies have employed the MRIO approach to calculate consumption-based emission for both CO_2[20,73] and air pollutants[22,23,30,76], and some studies have calculated pollution concentrations and health impacts associated with regions' export of goods[14,24].

Before decomposing to consumption-based emissions, the production-based emissions are aggregated from the 228 countries in our emission inventory to 129 GTAP regions and mapped from 62 sub-sectors in the inventory to 57 GTAP sectors. The residential sector is regarded as local direct consumption and thus not mapped to any GTAP sector. The region and sector mapping procedures are presented in Supplementary Table 1, 3 and 4.

After mapping to GTAP sectors and regions, for a given region c, its production-based emissions can be decomposed as:

$$E_{s,k,c} = \sum_{r=1}^{129} f_{k,r,c} E_{s,k,c} \qquad (3)$$

where s, k and r represent the species, economic sectors (here refer to 57 sectors in the MRIO) and consumption regions (here refer to 129 regions in the MRIO), respectively. $E_{s,k,c}$ represents total production-based emissions from sector k in region c. The coefficient $f_{k,r,c}$ represents the production (or output) fraction of sector k in region c related to consumption activities in region r, which is derived from the MRIO model presented below. Taking China as an example, Supplementary Fig. 4 demonstrated the fraction of China's production in each GTAP sector to the 129 regions.

Supplementary Fig. 5 compares the SO_2 emission intensity of the mineral products sector among the 13 regions. This figure reveals large regional disparity in emission intensity. For example, the highest intensity in China is about 20 times as much as that for Rest of East Asia

and Western Europe, due to regional differences in industrial and energy structure, energy efficiency, and emission control levels[14,25,28].

MRIO analysis is based on monetary flows between sectors and regions as:

$$\begin{pmatrix} \mathbf{x^1} \\ \mathbf{x^2} \\ \mathbf{x^3} \\ \vdots \\ \mathbf{x^m} \end{pmatrix} = \begin{pmatrix} \mathbf{A^{1,1}} & \mathbf{A^{1,2}} & \mathbf{A^{1,3}} & \cdots & \mathbf{A^{1,m}} \\ \mathbf{A^{2,1}} & \mathbf{A^{22}} & \mathbf{A^{2,3}} & \cdots & \mathbf{A^{2,m}} \\ \mathbf{A^{3,1}} & \mathbf{A^{3,2}} & \mathbf{A^{3,3}} & \cdots & \mathbf{A^{3,m}} \\ \vdots & \vdots & \vdots & \ddots & \vdots \\ \mathbf{A^{m,1}} & \mathbf{A^{m,2}} & \mathbf{A^{m,3}} & \cdots & \mathbf{A^{m,m}} \end{pmatrix} \begin{pmatrix} \mathbf{x^1} \\ \mathbf{x^2} \\ \mathbf{x^3} \\ \vdots \\ \mathbf{x^m} \end{pmatrix} + \begin{pmatrix} \sum_r \mathbf{y^{1,r}} \\ \sum_r \mathbf{y^{2,r}} \\ \sum_r \mathbf{y^{3,r}} \\ \vdots \\ \sum_r \mathbf{y^{m,r}} \end{pmatrix} \quad (4)$$

In matrix form, $\mathbf{x = Ax + y}$, where $\mathbf{x}^c$ is a vector of the total production (expressed as economic monetary output) of each sector in region c; $\mathbf{y}^{c,r}$ is a vector of the finished products by each sector produced in region c and consumed in region r; and $\mathbf{A}^{c,r}$ is a normalized matrix of intermediate coefficients in which the columns reflect the input from the sectors in region c required to produce one unit of production from each sector in region r.

Solving for total output, Eq. 4 can yield the following:

$$\mathbf{x = (I - A)^{-1}y} \quad (5)$$

where $(\mathbf{I\text{-}A})^{-1}$ is the Leontief inverse matrix, $\mathbf{I}$ is identity matrix, and $\mathbf{A}$ is the block matrix in Eq. 4. More detailed description of the MRIO approach can be found in previous literatures[73,75,77].

Under this MRIO framework, region- and sector- specific production (in 129 regions and 57 sectors) related to the consumption activity of a given region r can be calculated as:

$$\mathbf{x}_{com}^{\cdot r} = \mathbf{(I - A)^{-1}y^{\cdot r}} \quad (6)$$

where $\mathbf{y}^{\cdot r} = (\mathbf{y^{1,r}} \ldots \mathbf{y^{c,r}} \ldots \mathbf{y^{m,r}})'$ is a vector of the final consumption in region r and includes the final products produced in region r ($\mathbf{y^{r,r}}$) as well as products imported from other regions ($\mathbf{y^{c,r}}, c \neq r$). $\mathbf{x}_{com}^{\cdot r} = (\mathbf{x^{1,r}} \ldots \mathbf{x^{c,r}} \ldots \mathbf{x^{m,r}})'$ is a vector of the total productions of 129 regions for 57 sectors, which are related to consumption in region r. Thus the fraction of region- and sector-specific production ($\mathbf{f}^{\cdot r}$) related to consumption in region r can be calculated as:

$$\mathbf{f}^{\cdot r} = \mathbf{x}_{com}^{\cdot r}./\mathbf{x} \quad (7)$$

Consumption-based emissions are then derived by subtracting the exported and adding the imported emissions from regional total production-based emissions.

From both production and consumption perspectives, emissions for each of the 13 world regions are aggregated from emissions of all GTAP regions within that designated region. Supplementary Fig. 6 compares the production- and consumption- based emissions for each of 13 regions defined above. In general, consumption-based emissions are higher than production-based emissions in developed regions (opposite for developing regions), indicating that in net the developed regions have outsourced their pollutions to developing regions through international trade.

Estimates of production- and consumption-based PM$_{2.5}$ concentrations

The GEOS-Chem model was used to calculate fractional contribution of any given region's production- or consumption-related emissions to global PM$_{2.5}$ concentrations (Extended Data Fig. 7). Determined by the horizontal resolution of GEOS-Chem, the fractional contributions were determined on a 2º latitude × 2.5º longitude grid. These spatially-varying fractions were then multiplied by the 0.1º × 0.1º global annual mean PM$_{2.5}$ concentrations developed for GBD2013[27] to get estimate region's production- and consumption-based PM$_{2.5}$ concentrations; here each 0.1º × 0.1º GBD2013 grid cell is applied with the GEOS-Chem simulated fraction at the 2º × 2.5º grid cell that covers the high-resolution grid cell. The GBD2013 PM$_{2.5}$ data for 2007 were linearly interpolated from data for 2005 and 2010 that were estimated by combination of satellite-based estimates (MODIS, MISR, and SeaWiFS), chemical transport model simulations, and ground measurements[27].

Description of the base model simulation. GEOS-Chem is a global 3-dimensional model of the atmospheric compositions driven by the assimilated GEOS-5 meteorology (GMAO; http://gmao.gsfc.nasa.gov/). The model has a horizontal resolution of 2º × 2.5º and 47 vertical layers (with 10 roughly equal spaced layers below 850 hPa). The model was run with full O$_x$−NO$_x$−CO−VOC−HO$_x$ chemistry and includes sulfate-nitrate-ammonium[78,79], primary[80] and secondary[81] carbonaceous aerosols, mineral dusts[82,83] and sea-salts[84,85]. Sulfate-nitrate-ammonium is modeled by the ISOROPIA-II thermodynamical equilibrium. POA is simulated as primary organic carbon in the model and then multiplied by 1.8 to account for the oxygen molecules contained when calculating ambient PM$_{2.5}$ concentrations. Secondary organic aerosols (SOA) is predicted based upon rate constants and aerosol yield parameters determined from laboratory chamber studies[81,86]. The aerosol simulations have been extensively evaluated using ground-based measurements[79,82,87] and aircraft measurements[88,89].

The global anthropogenic emissions of NO$_x$, SO$_2$, CO, NH$_3$, BC and OC developed in this work were used to drive GEOS-Chem simulations. Annual emissions for each region were converted to monthly gridded emissions at 0.1º × 0.1º resolution in proportion to the monthly emissions grid maps of HTAP v2.2 for 2008[28]; these high-resolution emissions were automatically re-mapped to 2º × 2.5º in the model simulations.

Anthropogenic NMVOC emissions are taken from the monthly RETRO inventory with speciated NMVOC emissions[90]. In the case of the U.S. and Asia, the NMVOC emissions from RETRO are replaced by estimates from the regional inventories NEI05[38] and INTEX-B[57]. MEGAN emissions were used for biogenic NMVOC[91] and the monthly GFED3 dataset was used for the biomass burning emissions[92]. Other individual emission sources, such as aircraft[78], shipping[93], soil NO$_x$[94], and lightning NO$_x$[95-97], were also included in the simulation.

Model perturbation design to estimate regions' PM$_{2.5}$ contributions. Given the substantial computational expense of global GEOS-Chem simulations, we aggregated 129

GTAP regions into the 13 regions defined above and in Extended Data Fig. 1. The zero-out approach was used to simulate the fractional contributions of regions' production- or consumption-based emissions. In particular, a base simulation contains global anthropogenic and natural emissions (see above subsection). The first set of 13 scenarios separately subtracts the anthropogenic emissions of NO_x, SO_2, CO, NH_3, BC and OC produced within each of the 13 regions, to derive the contributions of the production-based emissions from each region to the global $PM_{2.5}$ concentrations. Similarly, the second set of 13 scenarios separately subtracts the consumption-based emissions of each region (by applying the fractions derived from Eq. 3) to estimate the contributions of each region's consumption to global $PM_{2.5}$ concentrations. Note that the emission fractions in Eq. 3 represent the emissions released in each GTAP region induced by consumption activities in all countries belonging to each of the 13 regions. For each case, emissions of residential sector are regarded as domestic consumption emissions are also removed from global total emissions. In all scenario runs, anthropogenic NMVOC emissions are held constant.

In all cases, the simulations were conducted for the entire year 2007 with a six-month spin-up starting from July 2006. The 24-h average $PM_{2.5}$ concentrations in the bottom layer of the model were taken to represent the ground-level concentrations.

Evaluation of the based model simulation. Both ground measurements and GBD $PM_{2.5}$ concentrations were used to validate the model-simulated $PM_{2.5}$ concentrations. Although there are a number of ground observation sites around the world, we only utilized the datasets from the National Air Pollution Surveillance network (NAPS; http://maps-cartes.ec.gc.ca/rnspa-naps/data.aspx) of Canada and the Interagency Monitoring of Protected Visual Environments network (IMPROVE; http://vista.cira.colostate.edu/improve/Data/data.htm) of the U.S. because only these two networks have relatively dense sites that can provide better representation of $PM_{2.5}$ concentrations within the $2^\circ \times 2.5^\circ$ grid. Locations of ground monitoring sites are presented in Supplementary Fig. 7 (a). Comparisons between the model simulations and the ground observations for Canada and the U.S. are presented in Supplementary Fig. 7 (b) and (c) respectively. In general, our modeled $PM_{2.5}$ concentrations agree well with IMPROVE observations in the U.S., but are biased high in comparison to NAPS observations in Canada. The linear relationship between our model results and observations support the reliability of our methodological approach, especially considering that the model output is only used to estimate the proportional contributions of regional production- and consumption-based emissions to global $PM_{2.5}$ concentrations.

Our simulated $PM_{2.5}$ chemical compositions (sulfate, nitrate, ammonium, BC and OC) are also evaluated using the observations from three regional networks, IMPROVE, European Monitoring and Evaluation Programme (EMEP; http://www.emep.int/) and East Asian Monitoring Network (EANET; http://www.eanet.asia/) for 2007. As shown in Supplementary Fig. 8, the modeled concentrations of these five species correlate relatively well with

observations (R^2 =0.52~0.78), but tend to underestimate BC and overestimate nitrate. The underprediction of BC may be explained by underestimate of BC emissions and the coarse resolution of the model[98]. In contrast, the overestimation of nitrate is probably due to excess HNO_3 production or insufficient inhibition of ammonia uptake by organic particle material, as investigated by previous studies[99-101].

Comparisons of modeled and GBD2013 PM$_{2.5}$ concentrations in the 13 regions are shown in Supplementary Fig. 9. The GBD2013 data are re-gridded from 0.1° × 0.1° to 2° × 2.5° for a consistent comparison. The two datasets agree reasonably well for most regions, with R^2 between 0.20 and 0.90. Where we discard grid cells that contain sparse human population (i.e. population density under 22.5 people/km^2 or the 25th percentile of population density globally) or have PM$_{2.5}$ concentrations dominated by dust (i.e. modeled fraction of dust exceeds 60%), the comparison of modeled and GBD2013 data improves, with R^2 increasing to between 0.35 and 0.96.

Discussion on nonlinearity and NMVOC. The zero-out approach used here may introduce additional bias due to the nonlinear relationship between emissions and modeled PM$_{2.5}$ concentrations. Here we used a reference scenario (nonanth) to evaluate such non-linear effects, by running the model with global anthropogenic emissions of NO_x, SO_2, CO, NH_3, BC and OC turned off. The biases from non-linear effects can then be estimated:

$$Bias = (base - nonanth) - \sum_{i=1}^{13}(base - case_i) \qquad (8)$$

where $case_i$ represents the set of 13 production- or consumption-based scenarios respectively. The absolute and relative biases of population-weighted mean PM$_{2.5}$ concentrations due to non-linear effects are presented in Supplementary Fig. 10. Across the 13 region, the absolute biases are -2.0 and +0.1 μg/m^3 and the relative biases are -12.0 and +1.4%, indicating that the biases related to non-linear effects are relatively small.

Finally, to quantify the impact of excluding anthropogenic NMVOC emissions from this emission-trade-health analysis, we conducted a sensitivity model run for consumption-based emissions of China by assuming the fraction of NMVOC emissions embodied in China's international trade is the same as BC (based on the rationale that the two have relatively similar sectoral contributions in emission inventories). As presented in Supplementary Table 5, the relative differences of regional PM$_{2.5}$ concentrations between including and excluding consumption-based NMVOC emissions in China are small (within ±2%).

PM$_{2.5}$ mortality estimates

We follow the methods of the GBD study to estimate the premature deaths from outdoor PM$_{2.5}$ exposure. The PM$_{2.5}$ concentrations obtained above were used in concentration-response functions derived from epidemiological studies in order to estimate the attributable premature deaths linked to each region's consumption or production. Our estimates include the impacts due to the four leading causes of deaths: ischemic heart disease (IHD), chronic obstructive pulmonary disease (COPD), stroke, and lung cancer (LC). We

used IER functions developed by Burnett et al. [2], which incorporated data from cohort studies of ambient $PM_{2.5}$ air pollution, household air pollution, and active and second-hand tobacco smoke, to describe the concentration−response relationship throughout the full distribution of ambient $PM_{2.5}$ concentrations (Eq. 9), including the high levels in China and India. For each disease, the relative risk (RR) for the mortality estimations for all-age group was calculated as[2]:

$$RR(C) = \begin{cases} 1 + \alpha \left(1 - e^{-\gamma(C-C_0)^\delta}\right), & if\ C > C_0 \\ 1, & else \end{cases} \tag{9}$$

where C is the annual mean $PM_{2.5}$ concentration (on a 0.1º × 0.1º grid) in 2007, which was linearly interpolated from data for 2005 and 2010 according to Brauer et al.[27] for GBD2013; C_0 is the counterfactual concentration; and α, γ, and δ are parameters used to describe the shape of the concentration-response curve which are obtained from Burnett et al. [2].

Premature deaths from total $PM_{2.5}$ exposures. The grid based (0.1º × 0.1º) premature deaths (D_i) attributable to total $PM_{2.5}$ exposures were then estimated:

$$D_i = \frac{RR-1}{RR} \times B \times P \tag{10}$$

where B is the regional level baseline incidence of a given health effect for all-age group derived from the GBD database (http://www.healthdata.org/gbd/data) and P is the size of the exposed population obtained from the LandScan global population database for 2008 at a 1 km resolution, which was further aggregated to the same resolution of the $PM_{2.5}$ concentrations (i.e. 0.1º × 0.1º).

Premature deaths from regional production and consumption. Due to the nonlinearity of the IER functions, the source-specific contribution to $PM_{2.5}$ mortality is non-uniform along the curve. Each source contributes a certain proportion to total $PM_{2.5}$ concentration, but we could not assume the contribution is located in distinctive intervals of concentration. Here, we used the direct proportion approach[102] to estimate the mortality contribution from each specific region's production and consumption. The direct proportion approach is based on an assumption that the contribution of one source to the disease burden of air pollution is directly proportional to its share of $PM_{2.5}$ concentration. This approach is insensitive to the order in which each source is removed from total concentration. It also has the advantage that the sum of mortality estimates from all sources equals the mortalities from ambient $PM_{2.5}$ exposure. The scientific basis of this assumption has recently been mathematically demonstrated in more recent GBD research, GBD MAPS[102]. Another GBD study that estimated deaths related to household cooking also chose the direct proportion approach to solve the non-linear problem[7].

For a given region, the premature deaths from its production or consumption can be calculated by multiplying its fractional contribution of production or consumption to $PM_{2.5}$ concentration to the total $PM_{2.5}$ related mortalities for each 0.1º × 0.1º grid cell (Eq. 11):

$$D_{pro/con} = D_i \times F_i = D_i \times \left(\frac{C_{base} - C_{pro/con}}{C_{base}}\right) \tag{11}$$

Where $D_{pro/con}$ is the grid-based premature deaths from the region's production or consumption; F_i is the GEOS-Chem modeled fractional contribution of PM$_{2.5}$ due to production or consumption in region i; $C_{pro/con}$ is the modeled PM$_{2.5}$ concentration from production- or consumption- based scenario defined above; C_{base} is the modeled PM$_{2.5}$ concentration from base case.

Comparison with other studies

The transboundary transport of PM$_{2.5}$ and its health impacts has been investigated by previous studies[12,13,18]. As a prominent example, the TF HTAP investigated the impacts of intercontinental transport of ozone and particulate matters on human mortality for North America, Europe, East Asia, South Asia, and Arctic with multi-model simulations[13,18]. There is a substantial discrepancy in health impacts from transboundary PM$_{2.5}$ pollution estimated by this work (411,100 deaths) and the HTAP (58,000).

However, these numbers do not reflect a good comparison of our results and those of the HTAP study. Such a comparison is challenging due to differences in methods, region definitions, and tagged species. For instance, HTAP and our analysis differ in study periods – the spatial distribution of emissions in 2007 (studied here) differs largely from the distribution in 2001 (in HTAP), as a result of rapidly decreasing (increasing) emissions in the developed (developing) countries between 2000 and 2007[35,104].

In particular, we believe domain definitions explain a large portion of the difference between our results and the HTAP. The spatial size of regions has an important effect. Larger domains imply fewer boundaries, and will therefore correspond to more deposition of PM$_{2.5}$ produced in a domain in the same domain and fewer deaths related to transboundary pollution. For example, we estimated 92,100 deaths in Europe due to transboundary PM$_{2.5}$ pollution, of which 64,300 deaths related to PM$_{2.5}$ transport between Western Europe and Eastern Europe. If Europe is instead modeled as a single large domain, the premature deaths in Europe due to transboundary PM$_{2.5}$ would decrease to 27,800.

In order to better compare our results to the HTAP study, we conducted a set of four GEOS-Chem runs which used our emission inventory but the same domain definitions as the HTAP, in turn reducing anthropogenic emissions in North America, Europe, East Asia, and South Asia by 20%. We then follow the same (GBD) approach to estimate health impacts of sulfate, BC, and OC (as in HTAP). Supplementary Table 6 shows the source-receptor relationships for concentrations of these three aerosol species for each of the four regions. Our model results are within or close to the ranges of multi-model simulations from HTAP, indicating that our results on transboundary transport of PM$_{2.5}$ are consistent with the HTAP study.

Supplementary Table 7 compares the transboundary health impacts as modeled in this sensitivity experiment with the results of the HTAP experiment. We estimated that 5% of total avoided deaths in the four regions were associated with transboundary pollution when cutting 20% anthropogenic emissions, very close to the HTAP estimates. However, our estimates for total avoided premature deaths are 2.8 times that of HTAP, due to differences in global total emissions and assumptions in mortality estimates (e.g., concentration-response functions).

We also compared our results with those of Liu et al.[12,98], which also investigated the intercontinental transport of fine aerosols and relevant heath impacts for ten regions using the MOZART-2 model. Considering the differences of model, emission inventory, and region definition, local contributions of sulfate derived by Liu et al.[98] and this work are generally comparable (Supplementary Table 8). Further comparison with Liu et al.[12,98] is not feasible due to differences in tagged sources and species, emission data, mortality rates, and concentration-response functions.

Uncertainties and limitations

Our results are subject to a number of uncertainties and limitations. The uncertainty ranges (95% confidence interval) in different steps of our analysis are discussed below.

First, estimates of air pollutant emissions are inherently uncertain due to incomplete knowledge of activity rates, technology distributions, and emission factors. Based on the propagation of error approach described above, we estimate uncertainty ranges of emissions estimates as presented in Supplementary Fig. 3. The uncertainties vary by species and region, with lower uncertainties associated with SO_2, NO_x, and CO emissions than BC, OC, and NH_3 emissions. Similarly, emissions uncertainty is less for developed regions than for developing regions. These ranges of uncertainty we estimate are consistent with the standard uncertainty ranges for different pollutants in previous studies[54] and are comparable to other global and regional inventories.

Second, using the MRIO model to allocate production-based emissions to the regions where goods and services are ultimately consumed introduces additional uncertainties, related to, for example, inconsistent statistics and sectoral mapping[105-107]. Intercomparison of different global MRIO models has shown that past estimates of global CO_2 emissions embodied in trade vary by up to 13%[108], and that the observed differences among MRIO results corresponds closely to differences in underlying production-based inventories, suggesting the uncertainty related to the MRIO model itself is relatively small. Supplementary Fig. 6 presents our estimates of uncertainty ranges pertaining to consumption-based emissions for each region, by adding a 13% of uncertainty to production-based emissions. As in the referenced intercomparison, these estimated uncertainties are slightly higher than that of production-based emissions.

Third, the $PM_{2.5}$ concentrations simulated by the global chemical transport model are affected by errors in emission inventories and the model representation of chemical and

physical processes such as deposition and scavenging, vertical transport, and secondary organic aerosols. The computational intensity of the GEOS-Chem model makes it infeasible to estimate related uncertainties by a sensitivity analysis that requires a large number of scenarios. Instead, we use the normalized root-mean-square deviation (NRMSD) between the modeled and the GBD $PM_{2.5}$ concentrations over populated regions (population density higher than 22.5 people/km^2) to represent the overall model errors for each region, considering the uncertainties of GBD annual mean $PM_{2.5}$ concentrations are around 5%[27]. As presented in Supplementary Fig. 9, the NRMSD varies by region, with lowest in Middle East and North Africa (9.9%) and highest in Western Europe (60.3%).

Fourth, the uncertainty in linking a given amount of $PM_{2.5}$ concentrations to premature deaths mainly comes from the statistical estimation and limited epidemiology evidence of the IER functions[1,2]. This uncertainty was quantified by 1,000 simulations using 1,000 sets of IER parameters. Simulations were conducted for each 0.1° × 0.1° grid cell and aggregated to 13 regions to obtain the errors in regional total $PM_{2.5}$ related deaths (Di). Uncertainty of GBD2013 $PM_{2.5}$ data is minor (5% on average[27]) compared to that of IER functions and ignored in the simulations.

As presented in Eq. 11, the overall uncertainties involved in regional production-based and consumption-based $PM_{2.5}$ related deaths are determined by uncertainties in GEOS-Chem simulated fractional contribution of $PM_{2.5}$ exposure (F_i) and in total $PM_{2.5}$ related death (Di) calculated by IER functions. We assume the NRMSD between the GEOS-Chem modeled and the GBD $PM_{2.5}$ concentrations to represent the errors in modeled $PM_{2.5}$ concentrations in the base case (C_{base}). Regional specific uncertainties from non-linear effects are derived from sensitivity analysis described above. We further assume an additional 13% for uncertainties related to the MRIO model for each consumption-based case[108]. The GEOS-Chem model related errors in scenario runs ($C_{pro/con}$) are estimated by adding these three uncertainties in quadrature. The errors in regional F_i were then quantified by 10,000 trails of Monte Carlo simulation. Uncertainty of Di follows the distribution generated by 1,000 sets of IER parameters. Finally, the overall uncertainties of production-based and consumption-based $PM_{2.5}$ related deaths were derived from aggregations of errors above.

From conducting a series of sensitivity tests, we found that the uncertainty in the parameters of the IER function is the largest contributor to the overall uncertainty, followed by uncertainty in chemical transport model that integrated the errors in chemical and physical processes and production-based emission inventories. Although the absolute errors in chemical transport models are large[109], most errors in base case and scenario runs are common and do not affect their relative differences (presented as F_i). The contributions from MRIO-related uncertainties in each consumption-based case (13%) and from nonlinearities from zero-out approach (within 10%) are relatively minor.

The robustness of our main findings can also be demonstrated by the broad consistency with previous studies. Our estimates on production-based emissions are generally consistent

with the HTAP v2.2 emission inventory[28] that represents the state-of-the-art understanding of global emissions. Our results on transboundary transport of $PM_{2.5}$ (ratios presented in Fig. 2a) are generally consistent with the HTAP study[13] when harmonizing the domain definition and targeted species. Our estimates of global mortality related to $PM_{2.5}$ pollution are very close to the GBD[1] and Lelieveld et al.[6].

The combined uncertainties do not account for all potential sources of uncertainty. For instance, the estimated death in Canada due to consumption in the U.S. may be biased because of many U.S. power plants are located near the border U.S.-Canada border and therefore may have been counted as Canada emission sources in the gridded inventory[28]. Similarly, the relatively coarse resolution of the global model will introduce additional errors when investigating population exposures (mainly in urban areas) although the base exposures are evaluated by the high-resolution GBD2013 $PM_{2.5}$ map. Although we do not attempt to quantify the related uncertainties, our results may also be affected by the inter-annual variability of climate and by changes in international trade, since it is performed for one specific year. These issues could be resolved in the future by performing high-resolution modelling for multiple years. In addition to uncertainties in parameters of the IER functions, the IER function itself also subjects to a number of limitations. The IER function assumes that at a given exposure level, toxicity is equivalent among all types of $PM_{2.5}$ exposure due to lack of information from epidemiological cohort studies[2], indicating that the estimated $PM_{2.5}$ exposure throughout the world has not been differentiated by the components or sources. However, for a region with specific pollution sources, the health consequences of $PM_{2.5}$ could differ from other regions due to the potential unequal toxicity of $PM_{2.5}$ from different sources. By assuming carbonaceous aerosols have a five times larger impact than inorganic aerosols, Lelieveld et al.[6] found that the sources of mortality attributable to $PM_{2.5}$ can differ significantly between different regions, especially in regions where carbonaceous aerosols have high contribution to ambient $PM_{2.5}$ (e.g., India), corroborating the importance of investigating differential toxicity of specific component species in future studies. The IER function also did not account for the temporal pattern of exposure and the interactions among different types of combustion, in which all need additional research in the future.

References

34 Lin, J. et al. Global climate forcing of aerosols embodied in international trade. Nature Geosci 9, 790-794 (2016).

35 EC-JRC/PBL, European Commission, Joint Research Centre (JRC)/Netherlands Environmental Assessment Agency (PBL). Emission Database for Global Atmospheric Research (EDGAR), release EDGAR version 4.2, available at: http://edgar.jrc.ec.europa.eu/ (last access: 15 December 2015), (2011).

36 Tsinghua University. Multi-resolution Emission Inventory for China, available at:

http://www.meicmodel.org (last access: 15 December 2015), (2015).

37 Li, M., *et al.* MIX: a mosaic Asian anthropogenic emission inventory under the international collaboration framework of the MICS-Asia and HTAP. *Atmos. Chem. Phys.* **17**, 935-963 (2017).

38 U.S. Environmental Protection Agency (USEPA). The 2008 National Emissions Inventory (NEI), release v3, available at: https://www.epa.gov/air-emissions-inventories/national-emissions-inventory (last access: 15 December 2015), (2013).

39 International Energy Agency (IEA). Energy Statistics and Balances of OECD Countries, 2007–2008, Paris, (2010a).

40 International Energy Agency (IEA). Energy Statistics and Balances of Non-OECD Countries, 2007–2008, Paris, (2010b).

41 Lu, Z., Zhang, Q. & Streets, D. G. Sulfur dioxide and primary carbonaceous aerosol emissions in China and India, 1996–2010. *Atmos. Chem. Phys*. **11**, 9839–9864 (2011).

42 Lu, Z. *et al*. Light Absorption Properties and Radiative Effects of Primary Organic Aerosol Emissions. *Environ. Sci. Technol.* **49**, 4868–4877 (2015).

43 Streets, D. G. *et al*. Anthropogenic and natural contributions to regional trends in aerosol optical depth, 1980–2006. *J. Geophys. Res.* **114**, (2009).

44 Streets, D. G. *et al*. All-Time Releases of Mercury to the Atmosphere from Human Activities. *Environ. Sci. Technol.* **45**, 10485–10491 (2011).

45 Amann, M. et al. Cost-effective control of air quality and greenhouse gases in Europe: Modeling and policy applications. *Environ. Model. Softw.* **26**, 1489-1501 (2011).

46 Yan, F., Winijkul, E., Jung, S., Bond, T. C. & Streets, D. G. Global emission projections of particulate matter (PM): I. Exhaust emissions from on-road vehicles. *Atmos. Environ.* **45**, 4830–4844 (2011).

47 Yan, F. *et al*. Global emission projections for the transportation sector using dynamic technology modeling. *Atmos. Chem. Phys*. **14**, 5709–5733 (2014).

48 Lu, Z. *et al*. Sulfur dioxide emissions in China and sulfur trends in East Asia since 2000. *Atmos. Chem. Phys*. **10,** 6311–6331 (2010).

49 Streets, D. G., Wu, Y. & Chin, M. Two-decadal aerosol trends as a likely explanation of the global dimming/brightening transition. *Geophys. Res. Lett.* **33**, (2006).

50 Streets, D. G. *et al*. Aerosol trends over China, 1980–2000. *Atmos. Res.* **88**, 174–182 (2008).

51 U.S. Environmental Protection Agency (USEPA). Compilation of Air Pollutant Emission Factors (AP-42), available at: http://www.epa.gov/ttn/chief/ (last access: 15 December 2015), (1999).

52 Habib, G. *et al*. New methodology for estimating biofuel consumption for cooking: Atmospheric emissions of black carbon and sulfur dioxide from India. *Global Biogeochem. Cy.*, **18**, (2004).
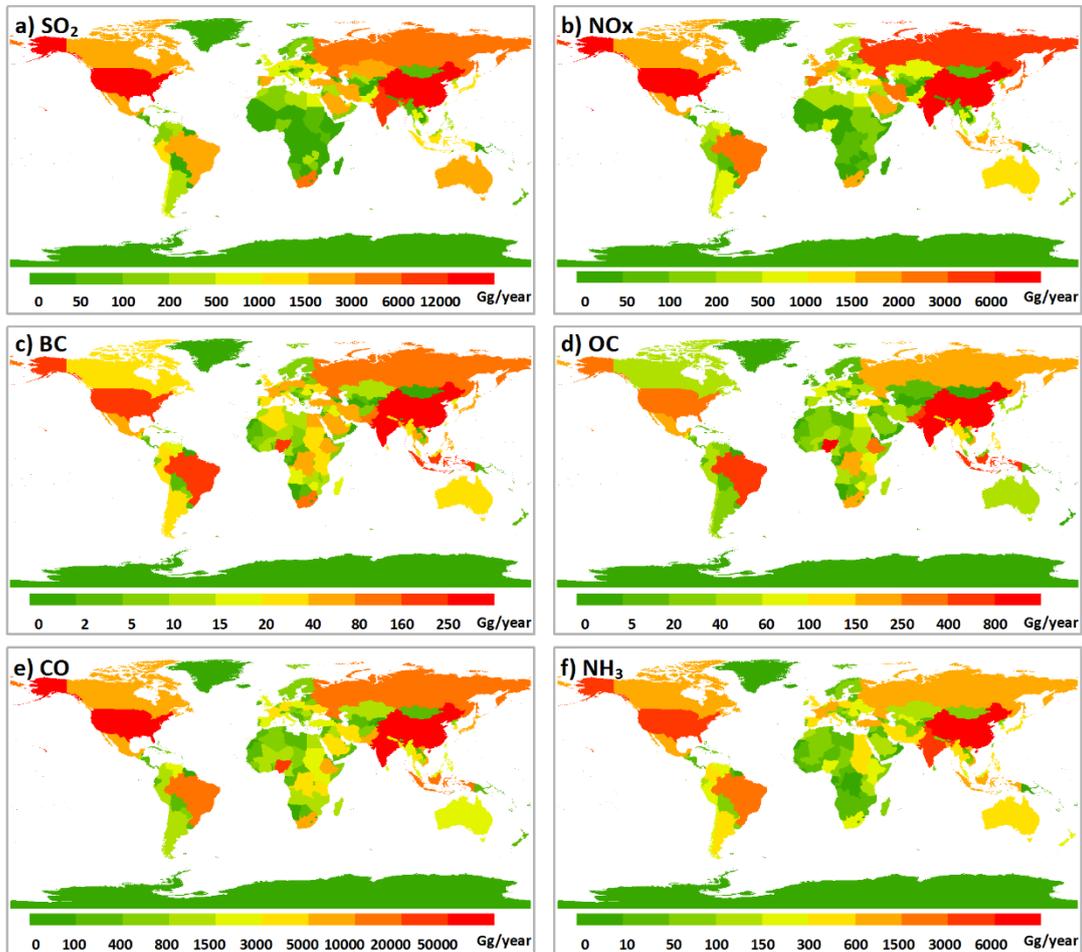
53 Gadi, R., Kulshrestha, U. C., Sarkar, A. K., Garg, S. C., & Parashar, D. C. Emissions of SO_2 and NO_x from biofuels in India. *Tellus B*, **55**, 787-795 (2003).

54 EMEP/EEA. EMEP/EEA air pollutant emission inventory guidebook 2013: Technical guidance to prepare national emission inventories, ISSN 1725-2237, EEA Techn. Report 12/2013, available at: http://www.eea.europa.eu/publications/emep-eea-guidebook-2013 (last access: 15 December 2015), (2013).

55 Streets, D. G. *et al*. An inventory of gaseous and primary aerosol emissions in Asia in the year 2000. *J. Geophys. Res.* **108**, (2003).

56 Zhang, Q. *et al*. NOx emission trends for China, 1995–2004: The view from the ground and the view from space. *J. Geophys. Res.* **112**, (2007).

57 Zhang, Q. *et al*. Asian emissions in 2006 for the NASA INTEX-B mission. *Atmos. Chem. Phys*. **9**, 5131–5153 (2009).

58 Lu, Z. & Streets, D. G. Increase in NO_x emissions from Indian thermal power plants during 1996–2010: unit-based inventories and multisatellite observations. *Environ. Sci. Technol.* **46**, 7463–7470 (2012).

59 Yevich, R. & Logan, J. A. An assessment of biofuel use and burning of agricultural waste in the developing world. *Global Biogeochem. Cy.* **17**, 4 (2003).

60 Kurokawa, J. *et al*. Emissions of air pollutants and greenhouse gases over Asian regions during 2000–2008: Regional Emission inventory in ASia (REAS) version 2. *Atmos. Chem. Phys*. **13**, 11019–11058 (2013).

61 European Monitoring and Evaluation Programme (EMEP). EMEP/CEIP 2014 Present state of emission data, available at: http://www.emep.int/ (last access: 15 December 2015), (2014).

62 Environment Canada. The National Pollutant Release Inventory (NPRI). available at: https://www.ec.gc.ca/ (last access: 15 December 2015), (2015).

63 Lei, Y., Zhang, Q., He, K. B. & Streets, D. G. Primary anthropogenic aerosol emission trends for China, 1990–2005. *Atmos. Chem. Phys*. **11**, 931–954 (2011).

64 Bond, T. C. *et al.* A technology-based global inventory of black and organic carbon emissions from combustion. *J. Geophys. Res.* **109**, (2004).

65 Bond, T. C. *et al*. Historical emissions of black and organic carbon aerosol from energy-related combustion, 1850-2000. *Global Biogeochem. Cy.* **21**, 2 (2007).

66 Lam, N. L. *et al.* Household Light Makes Global Heat: High Black Carbon Emissions From Kerosene Wick Lamps. *Environ. Sci. Technol.* **46**, 13531–13538 (2012).

67 Huang, Y. *et al.* Global organic carbon emissions from primary sources from 1960 to 2009. *Atmos. Environ.* **122**, 505-512 (2015).

68 Liu, F. *et al.* High-resolution inventory of technologies, activities, and emissions of coal-fired power plants in China from 1990 to 2010. *Atmos. Chem. Phys*. **15**, 13299-13317 (2015).

69 Lu, Z. and Streets, D. G.: The Southeast Asia Composition, Cloud, Climate Coupling Regional Study Emission Inventory, available at: http://bio.cgrer.uiowa.edu/SEAC4RS/emission.html (last access: 26 March 2014), (2012).

70 Zhao, Y., Nielsen, C. P., Lei, Y., McElroy, M. B., & Hao, J. Quantifying the uncertainties of a bottom-up emission inventory of anthropogenic atmospheric pollutants in China. *Atmos. Chem. Phys.* **11**, 2295-2308 (2011).

71 Zhao, Y., Wang, S., Nielsen, C. P., Li, X., & Hao, J. Establishment of a database of emission factors for atmospheric pollutants from Chinese coal-fired power plants. *Atmos. Environ.* **44**, 1515-1523 (2010).

72 Kuenen, J. J. P., *et al.* TNO-MACC_II emission inventory; a multi-year (2003–2009) consistent high-resolution European emission inventory for air quality modelling. *Atmos. Chem. Phys.* **14**, 10963-10976 (2014).

73 Davis, S. J., Peters, G. P. & Caldeira, K. The supply chain of CO_2 emissions. *Proc. Natl. Acad. Sci. USA* **108**, 18554-18559 (2011).

74 Wiedmann, T. A review of recent multi-region input–output models used for consumption-based emission and resource accounting. *Ecol. Econ.* **69**, 211-222 (2009).

75 Lenzen, M., Kanemoto, K., Moran, D. & Geschke, A. Mapping the Structure of the World Economy. *Environ. Sci. Technol.* **46**, 8374-8381 (2012).

76 Hertwich, E. G. *et al.* Integrated life-cycle assessment of electricity-supply scenarios confirms global environmental benefit of low-carbon technologies. *Proc. Natl. Acad. Sci. USA* **112**, 6277-6282 (2015).

77 Reis, S. et al. From Acid Rain to Climate Change. *Science* **338**, 1153-1154 (2012).

78 Park, R. J., Jacob, D. J., Field, B. D., Yantosca, R. M. & Chin, M. Natural and transboundary pollution influences on sulfate-nitrate-ammonium aerosols in the United States: Implications for policy. *J. Geophys. Res.* **109**, D15204, (2004).

79 Park, R. J., Jacob, D. J., Kumar, N. & Yantosca, R. M. Regional visibility statistics in the United States: Natural and transboundary pollution influences, and implications for the Regional Haze Rule. *Atmos. Environ.* **40**, 5405-5423 (2006).

80 Park, R. J., Jacob, D. J., Chin, M. & Martin, R. V. Sources of carbonaceous aerosols over the United States and implications for natural visibility. *J. Geophys. Res.* **108**, 4355 (2003).

81 Liao, H., Henze, D. K., Seinfeld, J. H., Wu, S. & Mickley, L. J. Biogenic secondary organic aerosol over the United States: Comparison of climatological simulations with observations. *J. Geophys. Res.* **112**, D06201 (2007).

82 Fairlie, D. T., Jacob, D. J. & Park, R. J. The impact of transpacific transport of mineral dust in the United States. *Atmos. Environ.* **41**, 1251-1266 (2007).

83 Zender, C. S., Bian, H. & Newman, D. Mineral Dust Entrainment and Deposition (DEAD) model: Description and 1990s dust climatology. *J. Geophys. Res.* **108**, 4416 (2003).
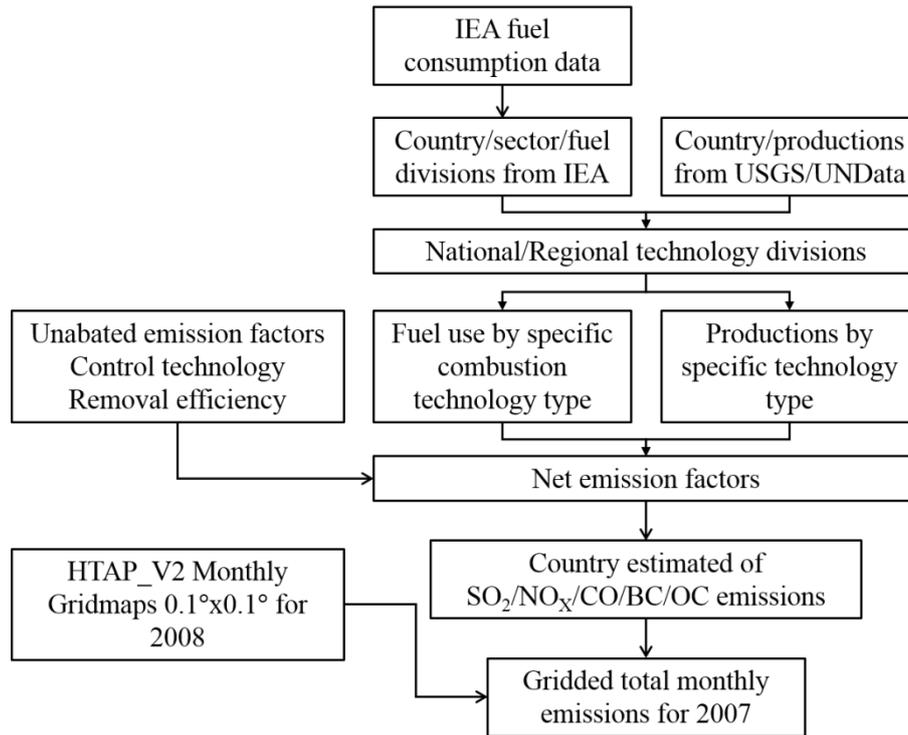
84 Alexander, B. *et al*. Sulfate formation in sea-salt aerosols: Constraints from oxygen isotopes. *J. Geophys. Res.* **110**, D10307 (2005).

85 Jaeglé, L., Quinn, P. K., Bates, T. S., Alexander, B. & Lin, J. T. Global distribution of sea salt aerosols: new constraints from in situ and remote sensing observations. *Atmos. Chem. Phys.* **11**, 3137-3157 (2011).

86 Seinfeld, J. H. & Pankow, J. F. Organic atmospheric particulate material. *Annu. Rev. Phys. Chem.* **54**, 121-140 (2003).

87 Pye, H. O. T. *et al*. Effect of changes in climate and emissions on future sulfate-nitrate-ammonium aerosol levels in the United States. *J. Geophys. Res.* **114**, D01205 (2009).

88 Heald, C. L. *et al*. A large organic aerosol source in the free troposphere missing from current models. *Geophys. Res. Lett.* **32**, L18809 (2005).

89 van Donkelaar, A. *et al*. Analysis of aircraft and satellite measurements from the Intercontinental Chemical Transport Experiment (INTEX-B) to quantify long-range transport of East Asian sulfur to Canada. *Atmos. Chem. Phys.* **8**, 2999-3014 (2008).

90 Bolshcer, M. *et al*. RETRO Deliverable D1-6. *RETRO Documentation* (2007).

91 Guenther, A. B. *et al*. The Model of Emissions of Gases and Aerosols from Nature version 2.1 (MEGAN2.1): an extended and updated framework for modeling biogenic emissions. *Geosci. Model Dev*. **5**, 1471-1492 (2012).

92 van der Werf, G. R. *et al*. Global fire emissions and the contribution of deforestation, savanna, forest, agricultural, and peat fires (1997–2009). *Atmos. Chem. Phys.* **10**, 11707-11735 (2010).

93 Wang, Y., Jacob, D. J. & Logan, J. A. Global simulation of tropospheric O_3-NO_x-hydrocarbon chemistry: 1. Model formulation. *J. Geophys. Res.* **103**, 10713-10725 (1998).

94 Yienger, J. J. & Levy, H. Empirical model of global soil-biogenic NOχ emissions. *J. Geophys. Res.* **100**, 11447-11464 (1995).

95 Murray, L. T., Jacob, D. J., Logan, J. A., Hudman, R. C. & Koshak, W. J. Optimized regional and interannual variability of lightning in a global chemical transport model constrained by LIS/OTD satellite data. *J. Geophys. Res.* **117** (2012).

96 Ott, L. E. *et al*. Production of lightning NOx and its vertical distribution calculated from three-dimensional cloud-scale chemical transport model simulations. *J. Geophys. Res.* **115** (2010).

97 Price, C. & Rind, D. Modeling Global Lightning Distributions in a General Circulation Model. *Mon. Weather Rev.* **122**, 1930-1939 (1994).

98 Liu, J., Mauzerall, D. L., Horowitz, L. W., Ginoux, P. & Fiore, A. M. Evaluating inter-continental transport of fine aerosols: (1) Methodology, global aerosol distribution and optical depth. *Atmos. Environ.* **43**, 4327-4338 (2009).

99 Heald, C. L. *et al*. Atmospheric ammonia and particulate inorganic nitrogen over the United States. *Atmos. Chem. Phys.* **12**, 10295-10312 (2012).

100 Walker, J. M., Philip, S., Martin, R. V. & Seinfeld, J. H. Simulation of nitrate, sulfate, and ammonium aerosols over the United States. *Atmos. Chem. Phys.* **12**, 11213-11227 (2012).

101 Kim, P. S. *et al.* Sources, seasonality, and trends of southeast US aerosol: an integrated analysis of surface, aircraft, and satellite observations with the GEOS-Chem chemical transport model. *Atmos. Chem. Phys.* **15**, 10411-10433 (2015).

102 GBD MAPS Working Group. Burden of Disease Attributable to Coal-Burning and Other Major Sources of Air Pollution in China. Special Report 20. Boston, MA: Health Effects Institute (2016).

103 World Health Organization, Review of evidence on health aspects of air pollution – REVIHAAP project, http://www.euro.who.int/__data/assets/pdf_file/0004/193108/REVIHAAP-Final-technical-report-final-version.pdf?ua=1 (WHO, 2013).

104 Klimont, Z., Smith, S. J. & Cofala, J. The last decade of global anthropogenic sulfur dioxide: 2000–2011 emissions. *Environ. Res. Lett.* **8**, 014003 (2013).

105 Wiedmann, T., Wilting, H. C., Lenzen, M., Lutter, S. & Palm, V. Quo Vadis MRIO? Methodological, data and institutional requirements for multi-region input–output analysis. *Ecol. Econ.* **70**, 1937-1945 (2011).

106 Steen-Olsen, K. *et al.* Accounting for value added embodied in trade and consumption: an intercomparison of global multiregional input–output databases. *Econ. Syst. Res.* **28**, 78-94 (2016).

107 Lenzen, M., Wood, R. & Wiedmann, T. Uncertainty analysis for Multi-Region Input-Output Models – a case study of the UK's carbon footprint. *Econ. Syst. Res.* **22**, 43-63 (2010).

108 Peters, G. P., Davis, S. J. & Andrew, R. A synthesis of carbon in international trade. *Biogeosciences* **9**, 3247-3276 (2012).

109 Lin, J. T. *et al.* Modeling uncertainties for tropospheric nitrogen dioxide columns affecting satellite-based inverse modeling of nitrogen oxides emissions. *Atmos. Chem. Phys.* **12**, 12255-12275 (2012).
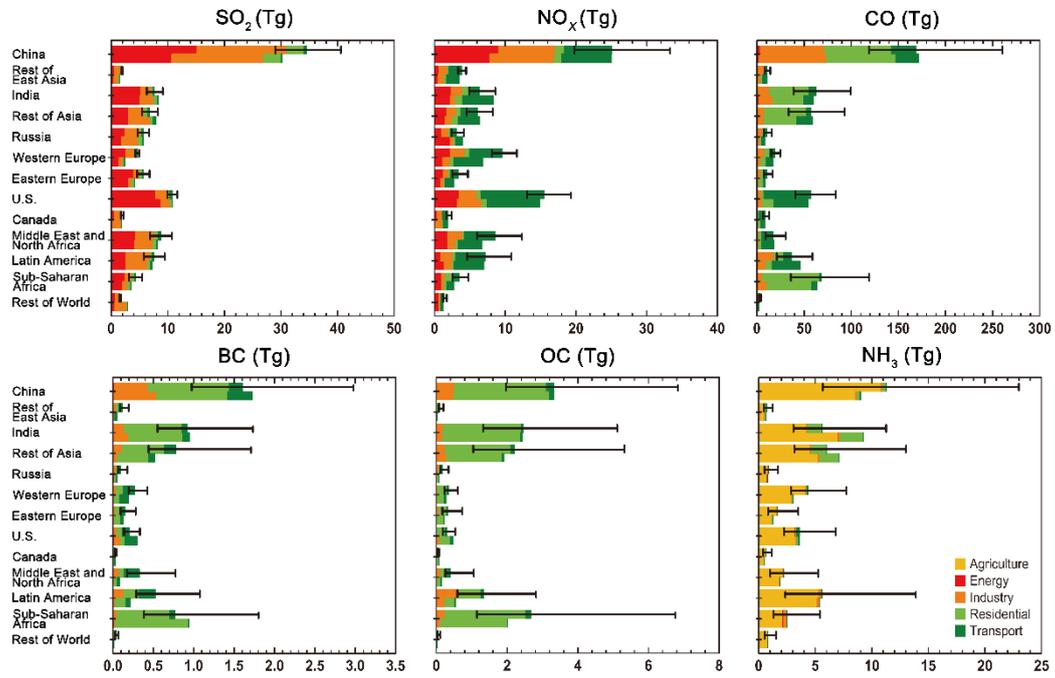
Supplementary Figure 1 | National annual production-based emission estimates in 2007 for each species: a) SO₂; b) NOₓ ; c) BC; d) OC; e) CO; f) NH₃.
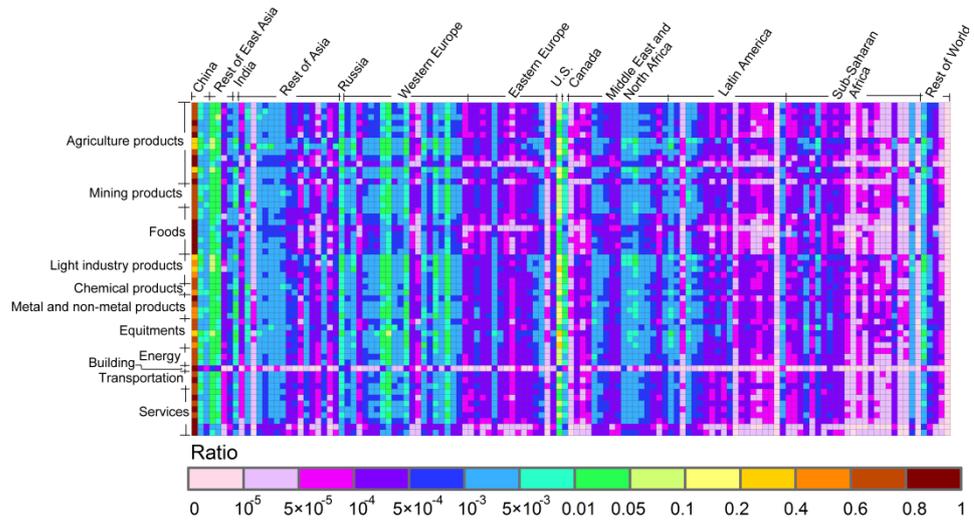
Supplementary Figure 2 | Schematic methodology for the development of the global production-based emission inventory.

```
                        ┌─────────────────────┐
                        │     IEA fuel        │
                        │  consumption data   │
                        └─────────┬───────────┘
                                  ↓
           ┌──────────────────────┐    ┌──────────────────────┐
           │ Country/sector/fuel  │    │  Country/productions │
           │  divisions from IEA  │    │   from USGS/UNData    │
           └──────────────────────┘    └──────────────────────┘
                        └───────────┬──────────────┘
                                    ↓
           ┌──────────────────────────────────────────────────┐
           │       National/Regional technology divisions      │
           └──────────────────────────────────────────────────┘
              ┌─────────────────────┼────────────────────┐
              ↓                     ↓                    ↓
┌──────────────────────┐ ┌──────────────────┐ ┌──────────────────────┐
│ Unabated emission    │ │ Fuel use by      │ │ Productions by       │
│ factors              │ │ specific         │ │ specific technology  │
│ Control technology   │ │ combustion       │ │ type                 │
│ Removal efficiency   │ │ technology type  │ │                      │
└──────────────────────┘ └──────────────────┘ └──────────────────────┘
              └───────────────────┐
                                  ↓
           ┌──────────────────────────────────────────────────┐
           │                Net emission factors               │
           └──────────────────────────────────────────────────┘
                                  ↓
┌──────────────────────┐ ┌──────────────────────────────────────┐
│ HTAP_V2 Monthly      │ │   Country estimated of               │
│ Gridmaps 0.1°x0.1° for│ │   SO2/NOX/CO/BC/OC emissions         │
│ 2008                 │ │                                      │
└──────────────────────┘ └──────────────────────────────────────┘
                   └──────────┐          ↓
                              ↓ ┌──────────────────────────────┐
                                │ Gridded total monthly        │
                                │ emissions for 2007           │
                                └──────────────────────────────┘
```

Flowchart boxes (top to bottom):

- IEA fuel consumption data
- Country/sector/fuel divisions from IEA
- Country/productions from USGS/UNData
- National/Regional technology divisions
- Unabated emission factors / Control technology / Removal efficiency
- Fuel use by specific combustion technology type
- Productions by specific technology type
- Net emission factors
- HTAP_V2 Monthly Gridmaps 0.1°x0.1° for 2008
- Country estimated of SO_2/NO_X/CO/BC/OC emissions
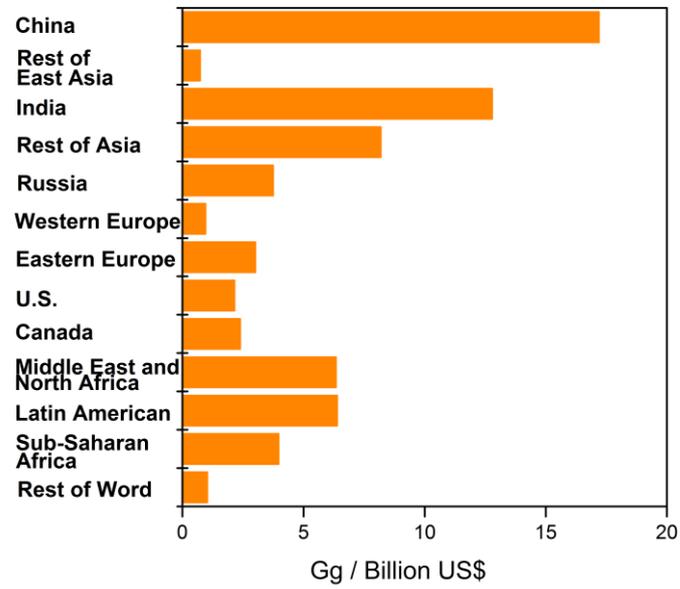- Gridded total monthly emissions for 2007

Supplementary Figure 3 | Comparison of production-based emission estimates between this work (2007) and HTAP v2.2 (2008) by sector and by region. In each panel, top and bottom bars represent emission estimates in this work and HTAP v2.2 respectively. Uncertainty ranges (95% CI) of emissions estiamtes in this work are also provided.
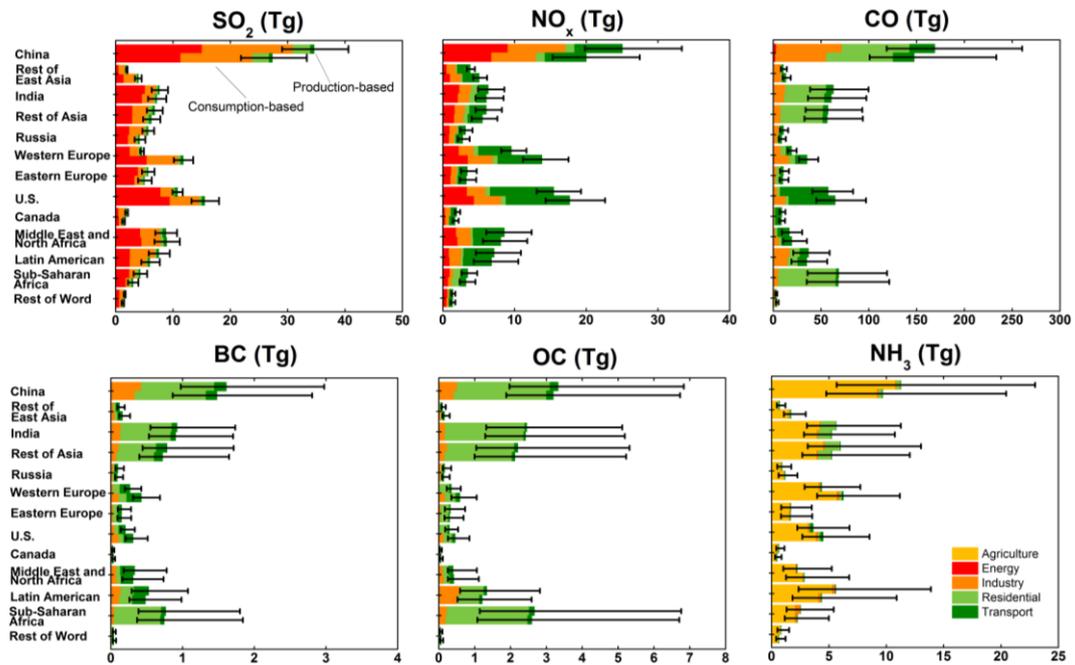
Supplementary Figure 4 | Fraction of China's production in each GTAP sector (from the top to the bottom) to the 129 regions (from the left to the right).
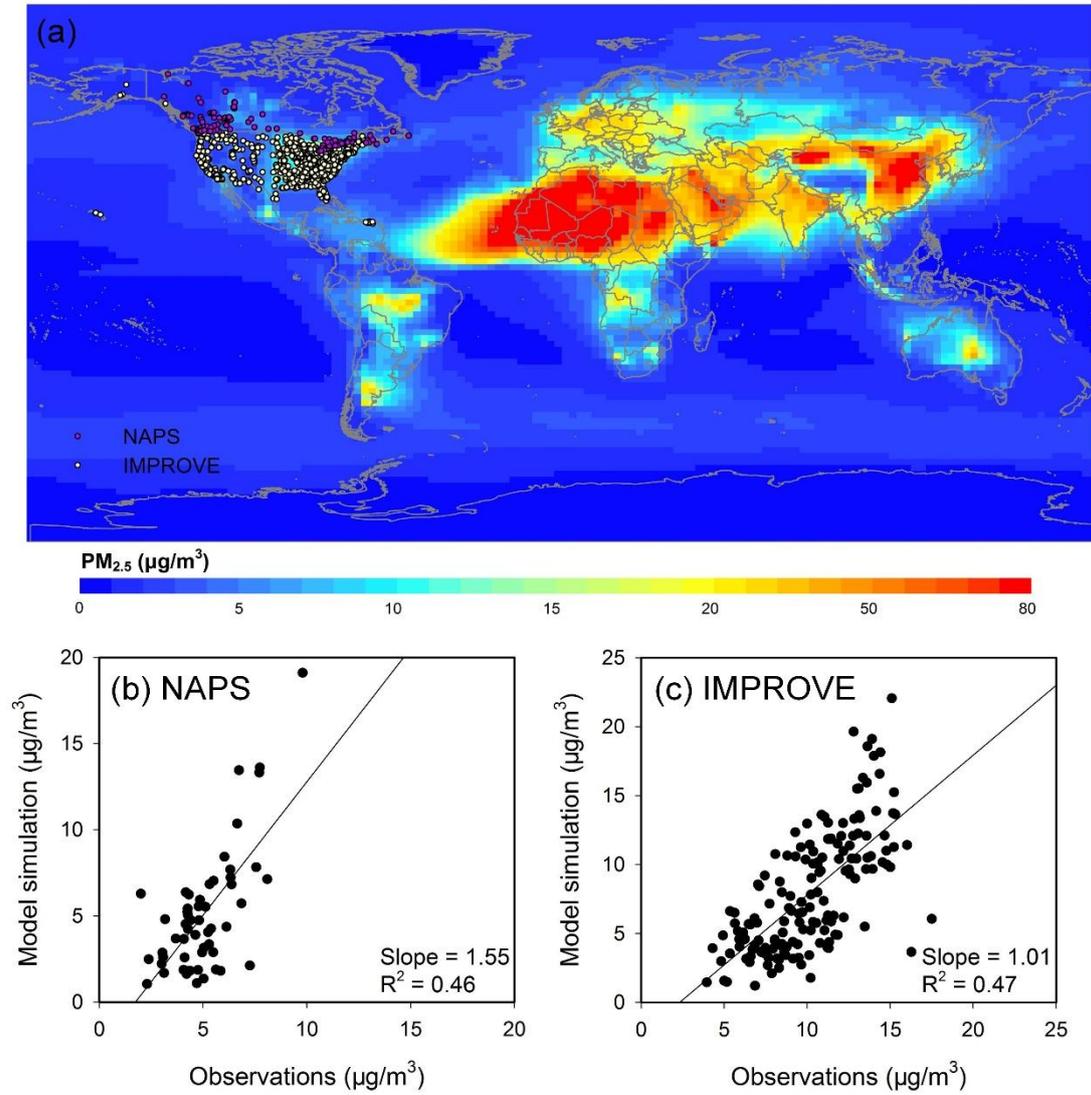
Supplementary Figure 5 | SO₂ emission intensity of mineral product sector in the 13 world regions
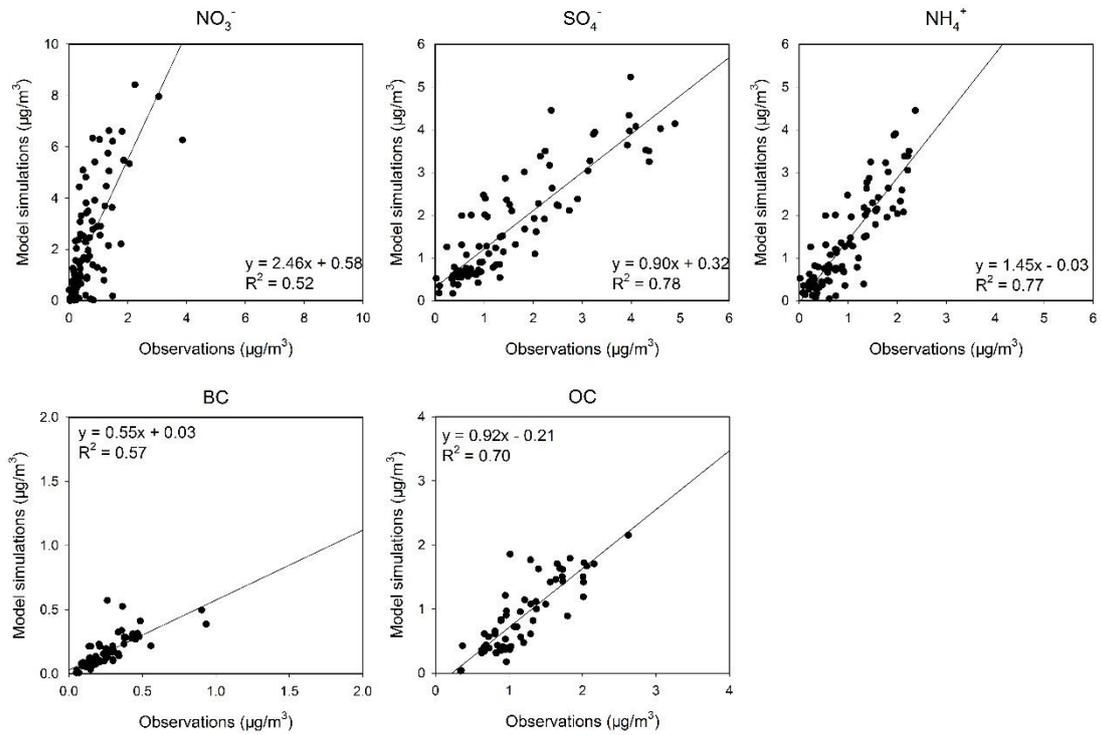

Gg / Billion US$

Supplementary Figure 6 | Comparison of production-based and consumption-based emissions for the 13 world regions. Uncertanty ranges (95% CI) of emissions estiamtes are presented.
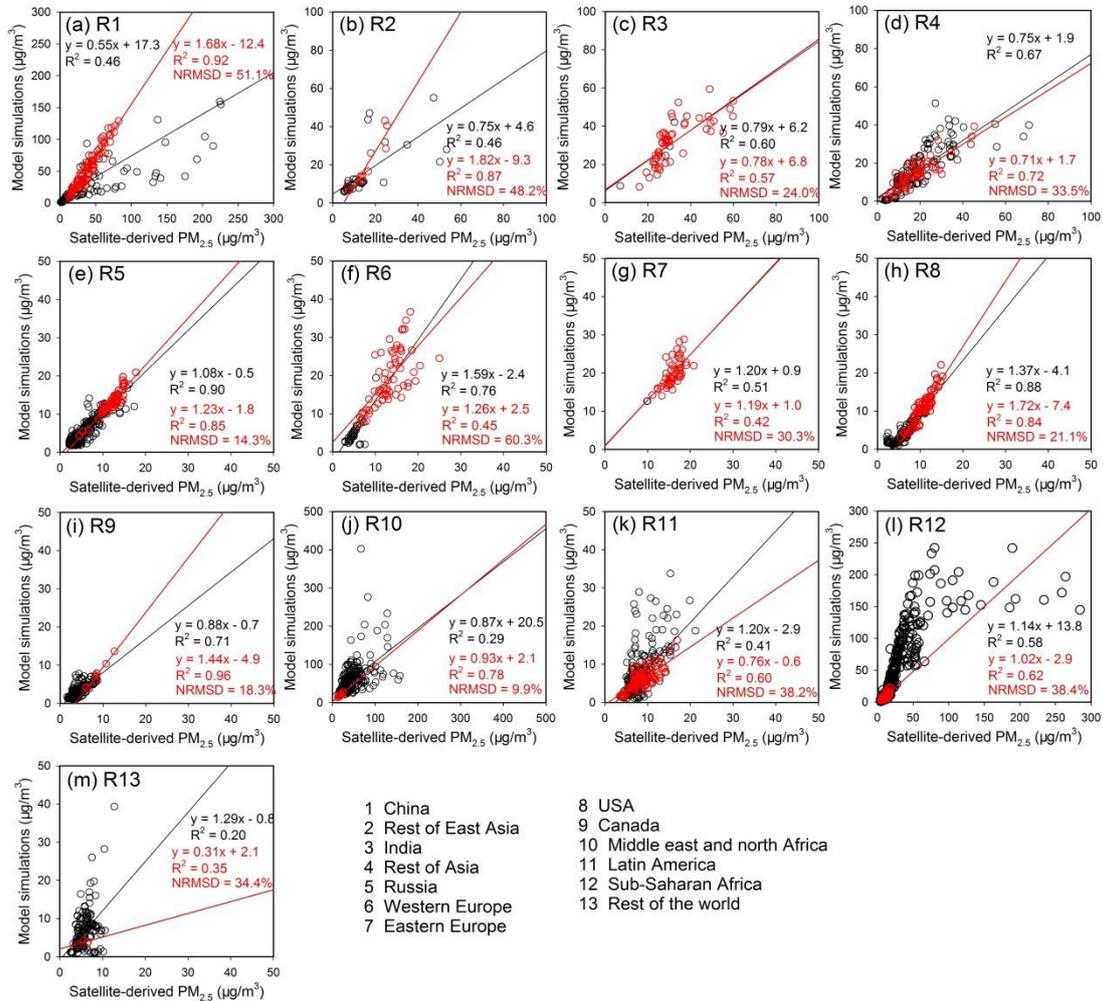
Supplementary Figure 7 | The annual averaged PM$_{2.5}$ concentrations of the base case from the GEOS-Chem model (a) and its comparison with the ground measurements in Canada (b) and the U.S. (c). The purple and yellow circles represent the spatial distribution of the NAPS and IMPROVE sites used in this study respectively.

Supplementary Figure 8 | Comparisons between the simulated and observed annual mean aerosol concentrations of nitrate, sulfate, ammonium, BC and OC. Measurements are taken from three regional networks (IMPROVE, EMEP and EANET).

NO_3^-: $y = 2.46x + 0.58$, $R^2 = 0.52$

SO_4^-: $y = 0.90x + 0.32$, $R^2 = 0.78$

NH_4^+: $y = 1.45x - 0.03$, $R^2 = 0.77$

BC: $y = 0.55x + 0.03$, $R^2 = 0.57$

OC: $y = 0.92x - 0.21$, $R^2 = 0.70$

Supplementary Figure 9 | Comparisons between the model simulated and GBD-based annual mean PM2.5 concentrations over 13 world regions. Those grids with dense population (population density above 22.5 people/km^2 or the 25th percentile of population density globally) and less affected by dust (modeled fraction of dust under 60%) are marked as red.

Supplementary Figure 10 | The absolute and relative biases of population weighted mean PM$_{2.5}$ concentrations for (a) production-based scenarios and (b) consumption-based scenarios due to non-linear effect.

Supplementary Table 5 | Changes in simulated ground-level PM$_{2.5}$ concentrations caused by the NMVOCs emissions for consumption-base scenario of China.

Receptor region	excluding NMVOC (μg/m^3)	including NMVOC (μg/m^3)	Relative difference (%)
China	34.06	33.86	-0.58
Rest of East Asia	6.19	6.17	-0.29
India	0.47	0.47	0.48
Rest of Asia	1.36	1.36	-0.07
Russia	0.44	0.44	-0.53
Western Europe	0.19	0.19	-0.04
Eastern Europe	0.18	0.18	-0.72
The U.S.	0.38	0.38	0.75
Canada	0.39	0.39	-0.10
Middle east and north Africa	0.13	0.13	-0.44
Latin America	0.17	0.17	0.85
Sub-Saharan Africa	0.05	0.05	1.58
Rest of the world	0.17	0.17	0.64

Supplementary Table 7 | Comparison of the inter-regional PM$_{2.5}$ health imapct with the HTAP study[13,18].

	Receptor (This study with HTAP domain)					Transport	
Source	NA	EA	SA	EU	World	death	fraction
NA	17651	225	174	1473	19973	2323	0.12
EA	666	234151	2285	1417	239942	5791	0.02
SA	61	1144	147609	891	151896	4287	0.03
EU	190	1666	3751	114029	127758	13729	0.11
Total	18567	237186	153819	117810	539569	26130	0.05
	Receptor (HTAP)					Transport	
Source	NA	EA	SA	EU	World	death	fraction
NA	9900	400	200	1200	11900	2000	0.17
EA	200	93400	900	400	95600	2200	0.02
SA	0	900	40000	100	41500	1500	0.04
EU	200	1600	1900	37400	43200	5800	0.13
Total	10300	96300	43000	39100	192200	11500	0.06

Supplementary Table 8 | Regional transport comparison with Liu et al. [98].

Receptors in Liu et al, 2009	Domestic SO_4^{2-} (%)		Region mapping with this study
	Liu et al, 2009	This study	
NA	83.5	40.5	The U.S. + Canada
SA	45.5	62.6	Latin America
EU	75.5	52.3	Western Europe + Eastern Europe
FSU	50.1	43.4	Russia
AF	18.8	36.2	Sub-Saharan Africa
IN	82.8	76	India
EA	85.3	76.1	China + Rest of East Asia
SE	43.4	34.4	Rest of Asia
AU	47.3	40.5	Rest of the world
ME	60.3	58.9	Middle east and north Africa